Int. J. Electrochem. Sci., 15 **(2020)** 9120 – 9134, doi: 10.20964/2020.09.02

International Journal of
ELECTROCHEMICAL
SCIENCE
www.electrochemsci.org

Corrosion Properties of Pure Aluminum Prepared by Spark Plasma Sintering (SPS) Using Different Grain Size of Aluminium Powders as Raw Material

Wenming Tian[1], Fangfang Chen[1,], Fasong Cheng[2], Zhonglei Li[1], Guoxing Pang[1]*

[1] School of Materials Engineering, North China Institute of Aerospace Engineering, No.133 Aimindong Road, Langfang Hebei Province 065000, China.
[2] AECC Guizhou Liyang Aviation Power CO.,LTD. Guiyang Guizhou 550014, China
[*]E-mail: 605917370@qq.com; tianwenming.dhr@163.com

Received: 17 April 2020 / *Accepted:* 5 June 2020 / *Published:* 10 August 2020

Five kinds of pure aluminum were prepared by spark plasma sintering using different grain size of aluminum powders as raw material. The effect of grain size on corrosion and passivation properties of these kinds of aluminum was investigated by potentiodynamic polarization, electrochemical impedance spectroscopy (EIS), Mott-Schottky test and immersion test. The results revealed that fine grain aluminum showed a bigger passive current density than those containing coarse grains. The corrosion current density at OCP also increased with decreasing grain size, indicating that the passive film formed on fine grains had a faster dissolution and repair rate. The pitting potential and the width of passive range increased with decreasing grain size. While, the defect density in passive film decreased with increasing grain size. The passive film formed on aluminum containing fine grains had superior protection performance against localized corrosion in general.

Keywords: A. Aluminum; B. Potentiodynamic; B. EIS; B. Mott-Schottky; B. Immersion test; C. Passive film

1. INTRODUCTION

Aluminum and its alloys are widely used in industry such as aerospace, construction, transportation, and machine manufacturing due to their excellent comprehensive properties, such as low density, high specific intensity and excellent corrosion resistance to atmospheric environment. However, the protective passive film formed on alloy surface will become vulnerable when aluminum is exposed to some aqueous solutions containing corrosive ions [1,2]. The main corrosion type of aluminum and its alloy in such aggressive environment is localized corrosion, because these aggressive ions can destroy the integrity of passive film and trigger localized dissolution of metal matrix [3-8]. Pure aluminum has

the best corrosion resistance in aluminum alloys and thus is usually used in the situations require strict corrosion resistance. The alloying elements and secondary phases play little role in the corrosion process of pure aluminum, while the grain boundary density could be a critical factor to influence corrosion properties. The aluminum atoms are randomly arranged at the grain boundary which leads to vacancy and dislocation in there, and thus corrosion preferentially nucleates at grain boundaries. Therefore, it is reasonable to expect that the variation in grain size will affect the corrosion performance of metals [9-20].

Various processing methods are adopted to alter the grain size of metals at present. For instance, severe plastic deformation (SPD) is a common way to improve the physical strength through grain refinement based on the Hall-Petch relation. In addition, the researches about the relations between grain size and corrosion rate are extensively performed [8,9]. Ralston [12] has studied the impact of grain size on corrosion of high purity aluminum with numerous grain refinement methods, including cold rolling, cold rolling, equal channel angular pressing (ECAP) as well as surface mechanical attrition treatment (SMAT). Nevertheless, it is unavoidable to generate many other physical changes in metal matrix, such as indices of lattice planes. it is also reported that SPD usually changes the deformation textures of metal matrix, residual stress and defect density which greatly affects the corrosion susceptibility of alloys. Song [10] found that in the ECAPed pure aluminum, amounts of high angle grain boundaries and intragranular dislocations provided more nucleation site to form a denser and thicker oxide film, and thus the ECAPed pure aluminum showed high corrosion resistance in aggressive environment. A higher density of matrix defects increases the rupture sites on passive films, but also accelerates the diffusion rate of atoms from lattice to passive film which benefits the maintaining of films. Therefore, the effect of traditional grain changing methods on corrosion is complicated. And the effect of grain size on corrosion is hard to decouple from other processing induced effects. Even the same grain size obtained by different process method will exhibit diverse corrosion properties and this issue may account for the non-ideal reproducibility of experimental data among many articles. The specialized study on relationship between grain size and corrosion response is still rare, limited by conventional processing methods.

Spark plasma sintering (SPS) technique, as a new kind of powder metallurgy (PM) technology, attracts lots of attention as soon as it appears. During the sintering course, sufficient electro-discharge between powders can generate local high temperature, causing the partial melting of powders surface, and the powders interior remains cold and solid. And in this way, the melted zone forms a new grain boundary, and each of the original powders eventually becomes a grain [21-23]. The SPS can prepare fully dense metals with a short sintering time and relatively low sintering temperature, and thus prevent the grain coarsening. Compared to SPD, the SPS can fully release the metal inner stress and does not change the texture of metals. Based on the above statements, SPS is the perfect choice to eliminate the interference of other influencing determinants while studying relevance between size of grain and corrosion behavior.

In this study, the small aluminum powder was used to simulate fine grain, and the big powder was used to simulate the coarse grain. The pure aluminum with different grain size was prepared by SPS. The relevant corrosion properties and passive performance of such aluminum were also characterized

by electrochemical tests. This study would develop a fundamental understanding about how grain size affects corrosion performance of pure aluminum.

2. EXPERIMENTAL

2.1. Specimen preparation

Five kinds of high purity aluminum powders with nominal diameters of 1 μm (*Φ*1), 5 μm (*Φ*5), 10 μm (*Φ*10), 20 μm (*Φ*20), and 50 μm were used to prepare the bulk metals. All aluminum powders (purity ≥ 99.9%, provided by HaoTian company) were produced by rotating disk centrifugal atomization. The SPS assembled aluminum specimens were named as AL1, AL5, AL10, AL20 and AL50 according to the size of their raw powders, respectively. These powders were firstly poured into a cylindrical graphite die with the inside diameter of 15 mm, and then put into the sintering furnace. The sintering temperature was 550 ºC with a heating rate of 50 ºC/min under vacuum. The holding time at 550 ºC was 1 min. A 60 MPa axial pressure was kept in the whole SPS process. The sintered samples were cooled naturally inside the furnace to room temperature. The total sintering time (including heating and cooling time) was about 30 minutes.

In order to observe the metallographic morphology of sintered aluminum, the bulk metal was mechanically ground with a series of emery paper from 600 to 6000 grit, then polished by 250 nm alumina spray suspension, and finally cleaned by deionized water and alcohol in turn. Prior to the observation, metals were etched by Keller's solution with a 10-30 s etching period. The sintered bulk aluminum was cut into 5×5×5 mm cube to immersion test and electrochemical measurements. The non-working surface of electrode was inlaid in epoxy resin. The working surface was treated by the same approach as the metallographic specimens.

2.2. Grain size characterization

The metallographic structure of sintered bulk aluminum was studied by Leica DM4000 metalloscope. Grain size of pure aluminum was semi-automatically determined from optical images, with the assistance of NanoMeasure software.

2.3. Electrochemical evaluation

All the electrochemical experiments were carried out in neutral 3.5 wt% NaCl solution using Corrtest CS350 electrochemical workstation. A three-electrode system was used for the tests, where a saturated calomel electrode (SCE) equipped with a Luggin capillary acted as the reference electrode, a platinum sheet acted as the auxiliary electrode.

Potentiodynamic polarization measurements were initiated at -150 mV referring to the open circuit potential (OCP) and scanned upwards with a 1 mV/s scanning rate until the current density reached 0.1 mA/cm^2. Electrochemical impedance spectroscopy (EIS) tests were performed at the OCP with a frequency range of 10 mHz to 100 kHz, under the load of a 10 mV AC excitation voltage. Mott-

Schottky tests were carried out at 10 mV AC stimulus signal at the frequency of 1 kHz, the test potential range was from open circuit potential to the pitting potential with a 20 mV/s scan speed. All the electrochemical experiments were repeatedly performed at least 3 times in order to obtain parallel valid data, and the running temperature of experiments was 25 ± 2 ^{o}C.

2.4. Morphological observation

The surface information of specimens after corrosion test was observed by RH-2000 three-dimensional video microscope. More detailed morphologies of corrosion were observed by JSM7500 scanning electron microscope in the secondary electron imaging (SEI) mode.

3. RESULTS AND DISCUSSION

3.1. Metallographic characterization of sintered aluminum

Fig. 1 shows the metallographic images of sintered aluminum with different grain size. Each original powder successfully turns to be an individual grain, and there exists remarkable distinction of grain size between five samples as shown in Fig. 1. Moreover, some defects like micro-pores or cavities that are common in as-cast metals, are rarely observed in sintered samples. It means that the sintered materials have extraordinary compactness. NanoMeasurer software was used to discretionarily measure 100 grains diameter, and the relevant results are shown by statistical histograms in Fig. 2. The grain size distribution of each sample is concentrated in a very narrow range. Table 1 shows the calculated average grain size as well as standard deviation from 100 selected grains of each sintered pure aluminum. Great correspondence between calculated size and nominal size reflects that the SPS technique indeed controls the dimension of powders during the sintering process. Therefore, it is reasonable to believe that the prepared samples meet the requirement in terms of grain size.

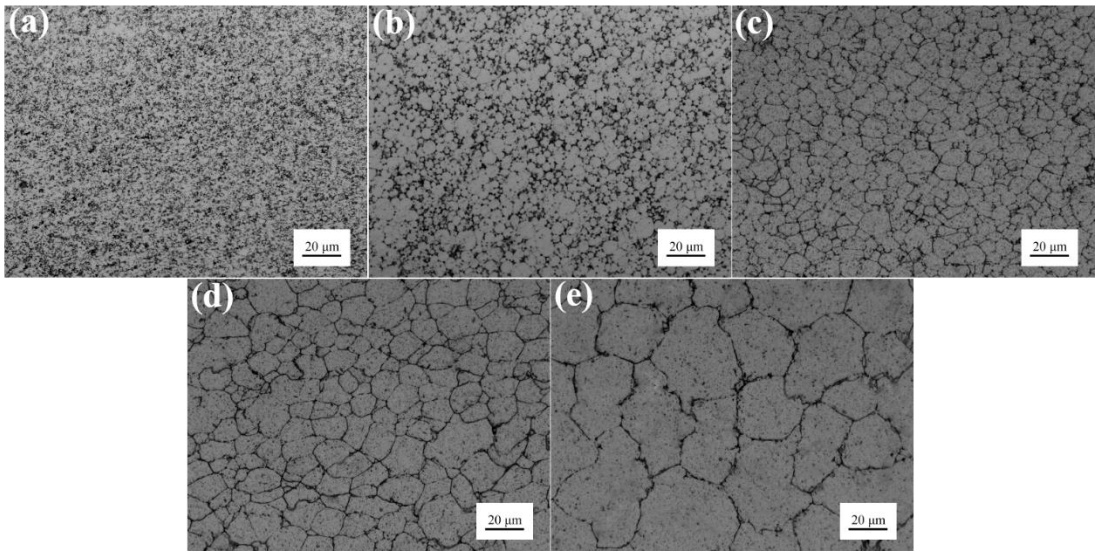

Figure 1. Typical metallographic optical images of sintered pure aluminum with different grain size: (a) AL1; (b) AL5; (c) AL10; (d) AL20; (e) AL50

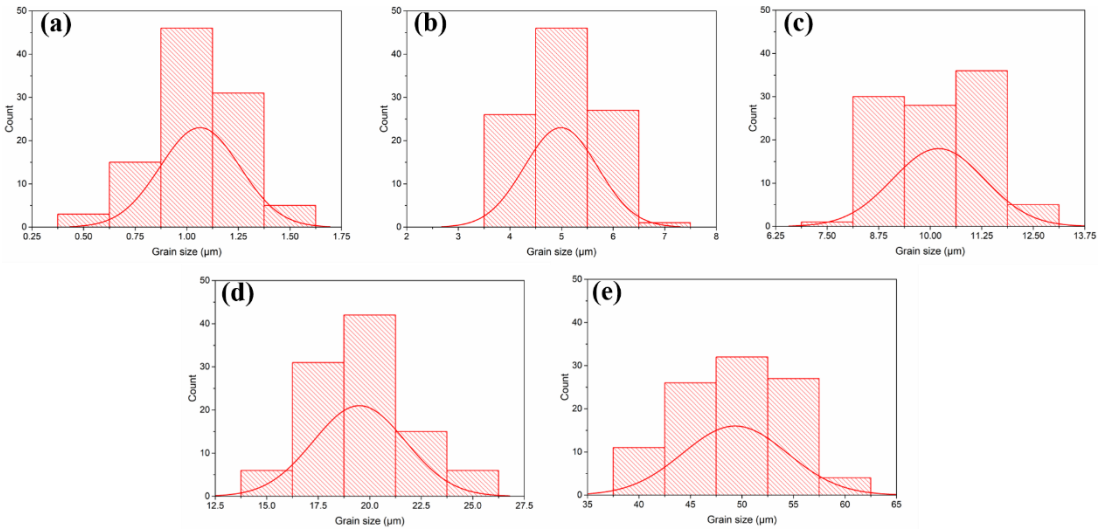

Figure 2. Grain size distribution histograms of sintered pure aluminum with different grain size: (a) AL1; (b) AL5; (c) AL10; (d) AL20; (e) AL50.

Table 1. Average grain size and standard deviation obtained by random statistics on 100 grains of metallographic micrograph.

Samples	Average grain size (μm)	Standard deviation (μm)
AL1	1.06	0.19
AL5	4.99	0.71
AL10	10.20	1.11
AL20	19.50	2.23
AL50	49.33	5.06

3.2. Potentiodynamic polarization test

In order to evaluate the corrosion resistance of five aluminum alloys, potentiodynamic polarization test is applied and the results are presented in Fig. 3. Even though the grain size of each aluminum is different, the cathodic branch of each single curve shows a similar shape, which indicates that the cathodic reaction of aluminum in neutral sodium chloride solution is usually an oxygen reduction and rarely affected by grain size. All of the samples exhibit typical passive behavior according to the polarization curves as the anodic current density showing tiny increase with applied potential. Obviously, the passive current density in anodic potential range increases with the decreasing grain size, indicating that a higher grain boundary density accelerates the dissolution/formation rate of passive film. Compared to the grain interior, gain boundary zone usually has a faster atom diffusion rate, and thus the aluminum with fine grains shows a bigger passive current density. The five kinds of pure aluminum also exhibit different corrosion potential (E_{corr}) and pitting potential (E_{pit}). in order to quantitatively evaluate the effect of grain size on metal corrosion, the Tafel extrapolation was used to analyze the polarization curves, and the relevant results are shown in Fig. 4. The error bar in Fig. 4 is derived from standard deviations of three parallel valid data.

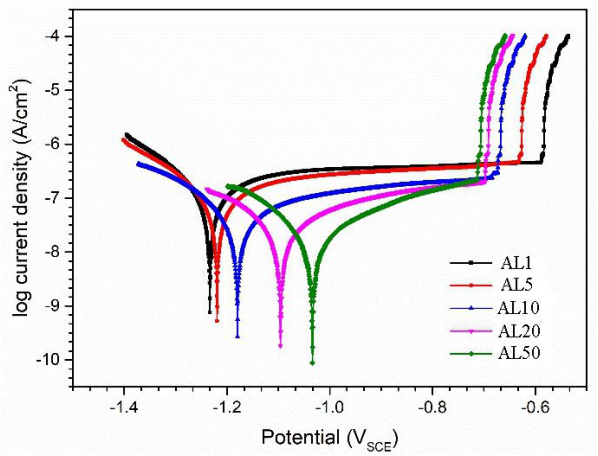

Figure 3. Potentiodynamic polarization curves of sintered pure aluminum after 1 h immersion in neutral 3.5 wt% NaCl solution

The corrosion current density at E_{corr} of aluminum decreases with increasing grain size, it means that coarse grains usually have a lower passive film dissolution rate at the native environment. The E_{corr} shows obvious increase with increasing grain size, indicating that the corrosion susceptibility of alloy also decreases with increasing grain size. As the vitally important parameters to estimate the corrosion resistance of materials, the increased E_{corr} and decreased i_{corr} with the coarsening grain implies that coarse grains are less sensitive to corrosion than fine grains at OCP during the 1 h immersion period. A smaller grain size means a higher density of grain boundaries, and thus more matrix defects for corrosion to nucleate and propagate. While, the E_{pit} increases with decreasing grain size, which is contrary to the E_{corr} changing trend. Therefore, the aluminum having a smaller grain size shows a wider passive potential range and thus a better passive ability and stability of surface oxide film. This can also be attributed to the higher grain boundary density which can accelerate the diffusion of aluminum ions out from metal matrix into oxide film, consequently, the oxide film has a faster repair speed [24-27].

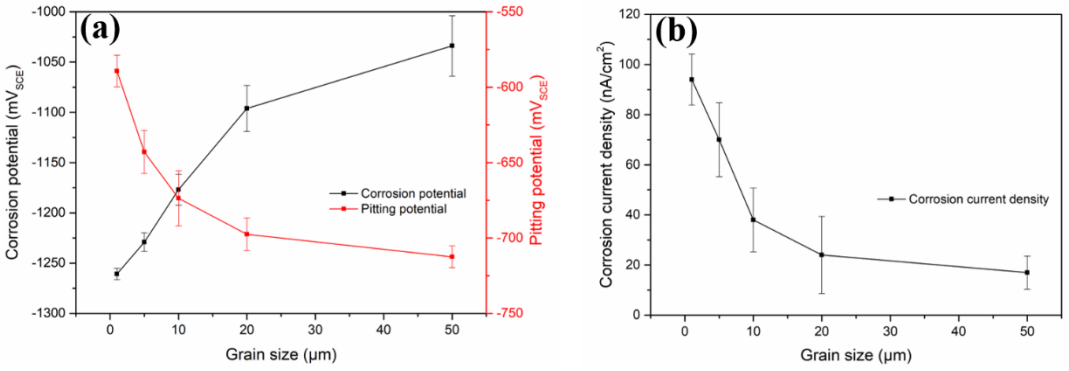

Figure 4. Values of (a) corrosion potential and pitting potential, (b) corrosion current density for five kinds of pure aluminum with different grain size

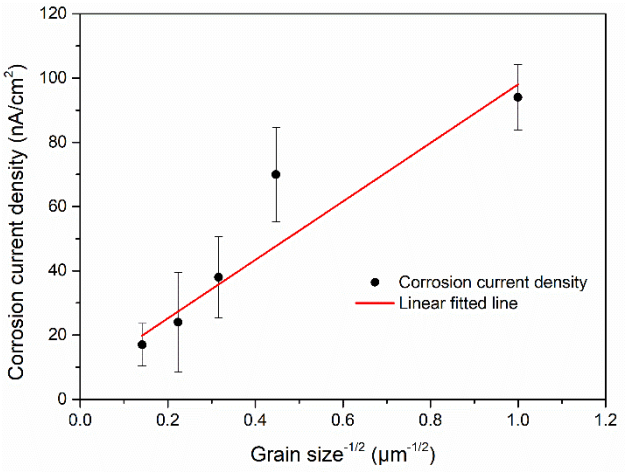

Figure 5. The relation between corrosion current density and grain size$^{-1/2}$ for pure aluminum with different grain size in neutral 3.5 wt% NaCl solution

Many researchers have attempted to identify the relation between grain size and corrosion rate, and eventually found that an analogous Hall-Petch relation may exist between grain size and corrosion rate [12,16,21,28]. Therefore, the relation between corrosion rate and $d^{-1/2}$ (d is the average grain size) was analyzed and linearly fitted. The Hall-Petch relation is definitely appropriate for the correlation between the i_{corr} and the $d^{-1/2}$ as shown in Fig. 5. Although the data of 5 μm aluminum somewhat deviate from the fitted line, the value of Adj. R-Square is 0.92002, proving that the fitted result has good reliability. The increasing grain size has two opposite effects on corrosion resistance of aluminum: one is reducing the grain boundary density thus improving the corrosion property of aluminum; and the other is deteriorating the repairing ability of passive film thus impairing the corrosion resistance of aluminum.

3.3. Electrochemical impedance spectroscopy measurement

The EIS tests are carried out in neutral 3.5 wt% NaCl solution after 1 h immersion to estimate the corrosion susceptibility of aluminum with different grain size. Fig. 6 shows the typical Nyquist plots of five kinds of samples. The Nyquist plots of samples AL1 to AL50 have the similar shape, i.e., the squished circular arcs. The straight line of 45-degree inclination representing the diffusion process does not appear at low frequency, and this means that the electrode system is only controlled by electrochemical reaction. The diameter of circular arc represents the charge transfer resistance, and increases with the increasing grain size, which indicates that the aluminum containing coarser grains has a lower dissolution rate of passive film.

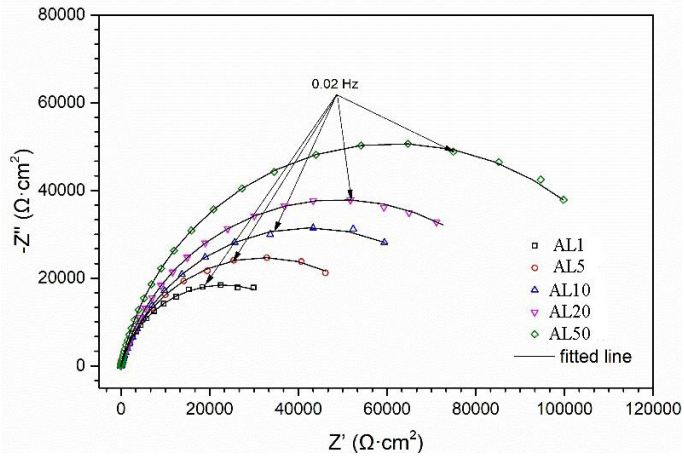

Figure 6. Typical Nyquist plots of EIS tests from five kinds of sintered pure aluminum with different grain size after 1 h immersion in neutral 3.5 wt% NaCl solution.

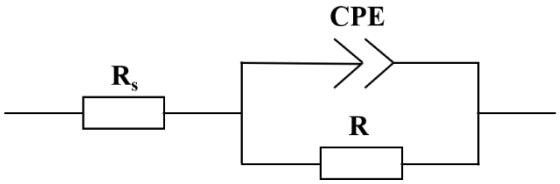

Figure 7. Equivalent electric circuit used to fit the Nyquist plots of the EIS measurements, R_s is solution resistance, CPE is constant phase element associated with the interface between pure aluminum electrode and solution, R is series resistance of charge transfer resistance and passive film resistance.

Table 3. Fitted values of parameters in equivalent electric circuit described in Figure 7 for sintered pure aluminum after 1 h immersion in neutral 3.5 wt% NaCl solution**.**

Samples	R_s ($\Omega \cdot cm^2$)	CPE		R ($\Omega \cdot cm^2$)
		Y ($\times 10^{-6}\ \Omega^{-1} \cdot cm^{-2} \cdot s^n$)	n	
AL1	1.26 ± 0.11	2.485 ± 1.243	0.745 ± 0.222	46034 ± 2348
AL5	1.43 ± 0.25	2.275 ± 1.103	0.799 ± 0.441	59713 ± 4180
AL10	1.66 ± 0.50	2.041 ± 0.490	0.813 ± 0.309	90706 ± 6349
AL20	1.15 ± 0.39	1.892 ± 0.795	0.842 ± 0.325	116389 ± 5005
AL50	1.59 ± 0.55	1.777 ± 0.355	0.875 ± 0.317	131817 ± 5272

In order to quantitatively investigate the EIS data, an equivalent electric circuit was used to fit the Nyquist plots, for its fitted error is very small (standard deviation $\chi^2 < 10^{-3}$). The equivalent electric circuit is shown in Fig. 7, including the elements defined as follows: R_s is the solution resistance, CPE is the constant phase element associated with the electric double layer and the passive film, and R is the series resistance of the charge transfer resistance R_{ct} and the passive film resistance R_{pf}, but the passive film is very thin, declaring that the value of R depends on that of R_{ct}. In this work, the constant phase

element replaces the capacitance, due to the dispersion effect on the aluminum electrode surface [29]. CPE in the equivalent circuit is actually the cascade of two constant phase elements representing electric double layer and passive film, respectively. The reason is that a compact passive film is formed on the surface of pure aluminum electrode, which means that a new phase, i.e., the passive film phase, is inserted between the metal matrix and the solution, and the so-called space charge layer will be generated in the passive film. The positive and negative charges will be concentrated on the two sides of the layer, respectively. And the impedance behavior of such layer corresponds to a constant phase element. Therefore, the space charge layer in passive film and the electric double layer in solution exist simultaneously between the metal matrix and the solution, and furthermore, the two layers are in series relationship.

Table 3 lists the fitted values of parameters in equivalent circuit, and the scatter bands are the standard deviations from 3 parallel valid data. The CPE of Table 3 consists of two parts: *Y* and *n*, which is defined as :

$$Z_{\mathrm{CPE}}(\omega) = [Y(j\omega)^n]^{-1} \qquad (1)$$

where *Z* is the impedance of CPE, *Y* is the magnitude of CPE, *j* is the imaginary number, $\omega = 2\pi f$ represents the angular frequency (*f* is the frequency in Hz), and *n* is the exponential term corresponding to the depression degree of the impedance spectra [30]. All the fitted values of parameters of Table 3 change regularly with the increasing of grain size, especially the value of *R* increasing prominently, implying a higher resistance to active dissolution (slower corrosion rate) in coarse grains. As previously mentioned, the main form of pure aluminum corrosion is localized corrosion. The corrosion initiates at feeble location of the passive film, and the formed metastable pits could be recovered by the repassivation of passive film [31,32]. Whereas, localized corrosion such as pitting propagation is most likely relevant to the active dissolution within the pit, for a high concentration of Cl^- and a low pH in pit cavity inhibit the repassivation, and thus the metastable pits gradually transform into the stable pits [33]. The results of *R* in EIS measurement are consistent with the results of E_{corr} and i_{corr} in potentiodynamic polarization test, demonstrating that the grain size definitely plays an important role in the active dissolution kinetics. According to the Hirschorn-Orazem theory, a formula applied to evaluate the effective capacitance is given as follows [34-38]:

$$C = Y^{\frac{1}{n}} R^{\frac{1-n}{n}} \qquad (2)$$

The values of *Y*, *n* and *R* in Table 3 are substituted into the formula to calculate the capacitance representing the electrochemical property of interface between aluminum matrix and solution phase. The calculated results of *C* as well as *R* are plotted in Fig. 8, in which the same variation trend as Fig. 4 is observed: the variation rate decreases with increasing grain size. As far as the analysis about electrochemical impedance spectroscopy is concerned, the effect of grain size on the corrosion resistance of aluminum is that high grain boundary density owned by fine grains makes it easy to dissolve actively. All the values of effective interfacial capacitance are extremely small and close to each other, because the space charge layer capacitance in passive film is only several microfarads per square centimeter (less than 10 $\mu F \cdot cm^{-2}$) and the Helmholtz electric double layer capacitance of aluminum reaches 30-50 $\mu F \cdot cm^{-2}$ based on the references, leading to that the effective series capacitance *C* becomes smaller than both of them [37,39-41].

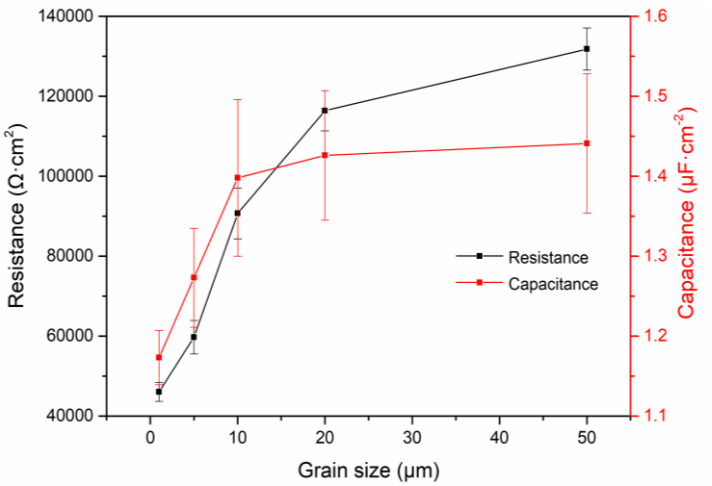

Figure 8. Values of series resistance R and effective capacitance C from five kinds of sintered pure aluminum with different grain size.

3.4. Mott-Schottky test

The pure aluminum has excellent corrosion resistance due to the presence of passive film. The electronic properties of film could strongly influence the corrosion behaviors of aluminum. Mott-Schottky test based on capacitance measurement is a powerful technique to assess the electronic properties of passive film. Due to the presence of space charge layers and voltage drops in the passive film, the characteristics of the defects in the film (density and type, etc.) are a function of the polarization potential. If the scanning potential changes fast enough (eg., more than 10 mV/s), the defect state in the passive film will be "frozen" and does not alter with the change of the polarization potential [37,41,42]. Meanwhile, why Mott-Schottky test can be used to analyze the semiconductor properties of the metal passive film is also based on such an assumption: the space charge layer capacitance of the passive film is much smaller than that of the double layer capacitance. At this time, the space charge layer capacitance of the film can determine the total interfacial capacitance. The space charge layer capacitance of passive film in the tested electrode system can be presented by the formula as follows [37,39-42]:

$$\frac{1}{C^2} \approx \frac{1}{C_{SC}^2} = \frac{2}{\varepsilon\varepsilon_0 q N_q}\left(E\text{-}E_{fb}\text{-}\frac{kT}{q}\right) \quad (3)$$

where C is the interfacial capacitance, C_{SC} is the space charge layer capacitance of the passive film, ε_0 is the vacuum permittivity, ε is the dielectric constant of the oxide film (which is confirmed as 10 for the value of aluminum oxide, Refs.[41,42], q is the elementary charge, N_q is the density of charge carriers, which represents the donor N_d for n-type and acceptor N_a for p-type semiconductor, respectively. E is the applied potential, E_{fb} is the flat band potential, k is the Boltzman constant, T is the Kelvin temperature. It can be known from the formula that the passive film capacitance is particularly sensitive to the density of the charge carriers. If there is no space charge layer in the passive film, there is no linear relationship between C^{-2} and E [39,40]. Fig. 9 shows the Mott-Schottky plots of the passive film on high purity aluminum with different grain size after 1 h stabilization of OCP in neutral 3.5 wt% NaCl solution. For a clear linear relationship only appears when the applied potential lies in the passive region, the plots selectively present the useful linear segments. The slopes of lines denoted as m can be used to calculate the N_q by the following equation:

$$N_q = \frac{2}{\varepsilon\varepsilon_0 q m} \quad (4)$$

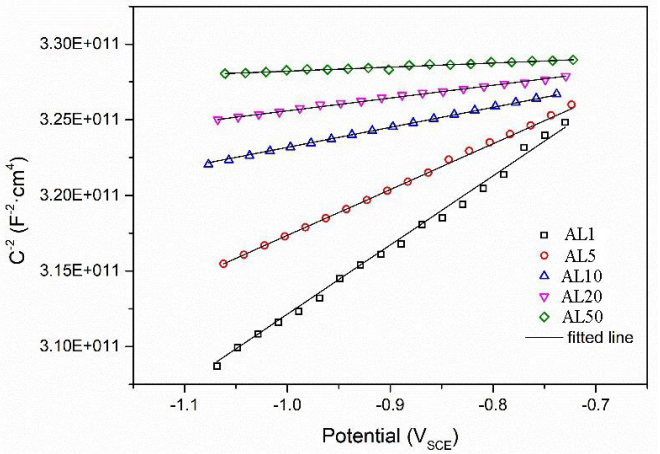

Figure 9. Linear segments of Mott-Schottky plots of the passive films formed on sintered pure aluminum with different grain size after 1 h immersion in 3.5 wt% NaCl solution

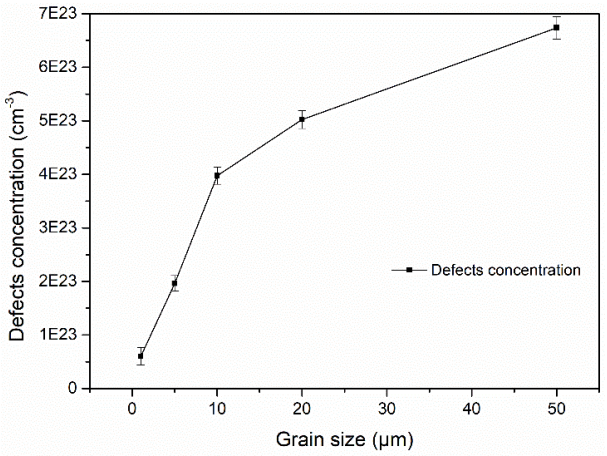

Figure 10. Values of the defects concentration N_d in passive film formed on five kinds of pure aluminum with different grain size.

In Fig. 9, the capacitance decreases with increasing grain size, which seems to contradict the results of EIS, and this is actually due to the interference of electric double layer capacitance, for the capacitance of EIS is the series capacitance of passive film capacitance and electric double layer capacitance. Besides, the linear segments with positive slopes suggest that all the passive films formed on the sintered high purity aluminum behave as n-type semiconductors, so the N_q is the donor density N_d. According to Eq. (4), the calculated values of N_d are plotted in Fig. 10, and the error bars in the plots are the standard deviations from 3 parallel valid data. The magnitude of N_d values (10^{22} -10^{23} cm^{-3}) is indicative of the highly disordered characteristic of the passive films formed on the surface of the pure aluminum. The values of N_d increase notably as the grain size increased, and such difference in N_d is connected with the stability of passive films. The N_d in general, corresponds to the defects in the passive film, whose difference reveals the variations in electronic structure of the passive films [45]. For an n-

type passive film, the defects should be the predominant oxygen vacancies V_o and interstitial aluminum cations Al_i^{3+}, and both of them are electron donors. These defects as the charge carriers govern the transport of ions through the passive films and penetration of Cl^- through the passive film. Since Cl^- penetration always takes place through these defects and consequently results in breakdown of the passive film. A smaller N_d usually means a higher stability of the passive film. As far as the analysis about the Mott-Schottky plots is concerned, it can be concluded that the fine grains prompt the pure aluminum to generate a more stable passive film and hence are more resistant against localized corrosion than the coarse grains. The conclusion is in accordance with the potentiodynamic polarization results in terms of the pitting potential.

3.5. Corrosion morphology observation

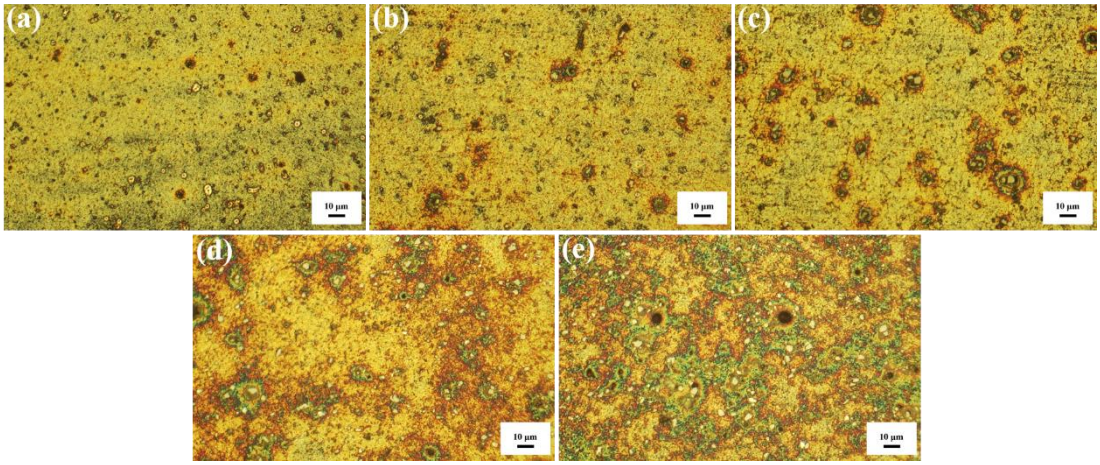

Figure 11. Typical corrosion morphologies of pure aluminum with different grain size: (a) AL1, (b) AL5, (c) AL10, (d) AL20, (e) AL50, after 20 days immersion in neutral 3.5 wt% NaCl solution.

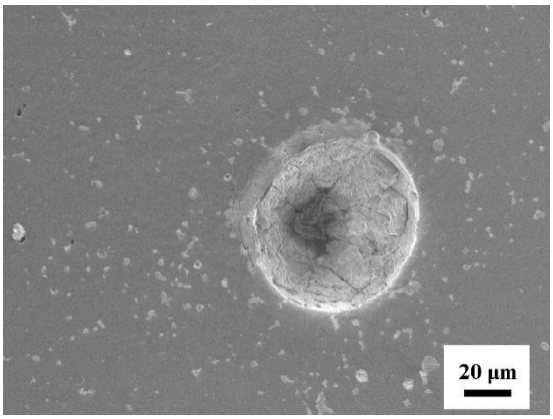

Figure 12. SEI image of typical pit in the sintered pure aluminum after 20 days immersion in neutral 3.5 wt% NaCl solution.

In order to investigate the difference of natural corrosion behaviors on pure aluminum samples, a conventional immersion test is applied and the corrosion morphology of specimens after 20 days

immersion is shown in Fig. 11. Fig. 11 shows the pits caused on the surface of aluminum during immersion tests, reflecting that the pitting corrosion definitely occurs on all pure aluminum samples. However, by the measurement of three-dimensional video microscope, the depth of these pits is very shallow (only 1 to 3 μm), and the difference of pit depth is far less than that of pit area on five kinds of sintered aluminum samples, which indicates that the specimens still belong to the stage of pitting initiation stage, and the existing pits have not enough time to propagate into the deep inner of pure aluminum matrix. Hence, the corrosion resistance against Cl^- ion in aggressive environment mainly depends on the protection performance of passive film. Table 4 is the statistical values of average pit mouth diameter and pit area from five kinds of samples, analyzed by the 2D measurement software of RH-2000 three-dimensional video microscope. It clearly shows that with increasing grain size, the distribution of pits becomes continuous, especially in Fig. 11e: the pits are linked together to form a corrosion network. The values of average pit mouth diameter and pit area concretely prove the poor barrier property of passive film on the coarse grain samples. And it is reasonable to deduce that the stability of passive film is the dominant factor during the initiation process of pitting. The result is in agreement with that of Mott-Schottky test, and it further confirms that the high defects density of coarse grains makes the passive film vulnerable to the corrosive ions, and thus pits will initiate at these defects. Fig. 12 is the secondary electron image (SEI) of typical pits in the sintered high purity aluminum, which shows more details of the typical pit: the pit is an inverted cone with an uneven inner surface. By the way, the difference of defects density mainly derives from the variation in grain size, and the higher the density of grain boundary, the lower the defects density, which is demonstrated not only in this work, but also in other references [10,17,28].

Table 4. Statistical values of average pit mouth diameter and pit area of corrosion pit formed on pure aluminum with different grain size after 20 days immersion in neutral 3.5 wt% NaCl solution.

Samples	Average pit mouth diameter (μm)	Pit area (μm^2)	Pit area ratio (%)
AL1	3.90 ± 1.96	1457.07 ± 16.14	6.32 ± 0.07
AL5	5.33 ± 3.14	1945.56 ± 20.75	8.44 ± 0.09
AL10	7.21 ± 5.97	3661.54 ± 50.69	15.89 ± 0.22
AL20	13.42 ± 6.35	5689.30 ± 221.21	24.69 ± 0.96
AL50	27.10 ± 10.54	8916.97 ± 373.27	38.70 ± 1.62

4. CONCLUSION

In this work, the high purity aluminum with different grain size were prepared by spark plasma sintering. The relevant corrosion properties of aluminum were also investigated, the corrosion and passive properties were strongly dependent on grain size.

(1) SPS truly could prepare fully dense aluminum. The grain size was almost the same to the original powder diameter.

(2) Polarization results show that the E_{corr} increases and the i_{corr} decreases with the increasing

grain size, indicating that the passive film formed on coarse grains have a low dissolution rate. Fine grain pure aluminum has a bigger passive current density. The E_{pit} and the width of passive range both increased with the decreasing grain size, indicating that the passive film formed on fine grains had a faster dissolution rate but a faster repair rate, and thus shows better protection.

(3) EIS analysis revealed that the R representing the synergy of charge transfer resistance. And corrosion resistance increased with the increasing grain size. The low grain boundary density of coarse grains makes it hard to cause active dissolution during corrosion, the passive film formed on coarse grains showed a slower dissolution rate.

(4) Mott-Schottky test revealed that the passive film formed on the surface of pure aluminum was a n-type semiconductor. The defects density N_d increases with the increasing grain size, further confirming that the grain size can affect the protective properties of passive film by altering the defects density in the passive film. Passive film formed on fine grains showed a better protectiveness.

(5) Immersion test indicated that the average pit mouth diameter and pit area increased with increasing grain size. The corrosion morphology was strongly dependent on passive film properties. The passive film formed on fine grains was more stable than that on coarse grains, and the result was similar to that of the pitting potential as well as the Mott-Schottky test.

ACKNOWLEDGEMENT
This research is sponsored by the Youth Fund of the Hebei Natural Science Fund project under Grant No. E2019409052, and the Education Department Science Research project of Hebei under Grant No. QN2019104.

References

1. D. Li, Z. Shi, H. Xu, Y. Chen, W. Feng, Z. Qiu, H. Liu, G. Lv, S. Wang, and Y. Fan, *Int. J. Electrochem. Sci.,* 14 (2019) 3465.
2. Q. Zhao, J. Zhao, C. Guo, H. Wang, Y. Huang, X. Cheng, and X. Li, *Int. J. Electrochem. Sci.,* 14 (2019) 8228
3. J. Weissenrieder, C. Leygraf, M. Gothelid, and U. O. Karlsson, *Appl. Surf. Sci.,* 218 (2003) 155.
4. D. Zhang, J. Xia, Q. Yang, T. Wei, L. Gong, and S. She, *Int. J. Electrochem. Sci.,* 15 (2020) 1072.
5. Z. Zhang, Z. Xu, J. Sun, M. Zhu, Q. Yao, D. Zhang, and B. Zhang, *Int. J. Electrochem. Sci.,* 15 (2020) 1218.
6. V.A. Arizmendi-Salgado, S.A. Serna, A. Torres-Islas, R. Soto-Espitia, P. Althuzer, S. Mejia-Sintillo, J. Campos-Alvarez, and J.G. Gonzalez-Rodriguez, *Int. J. Electrochem. Sci.,* 14 (2019) 8243.
7. D. Ortega, C. Alvarado, L. Muñoz, H. Kohler, F. Pineda, M. Páez, M. Sancy, N.D. Vejar, and J.M. Blamey, *Int. J. Electrochem. Sci.,* 14 (2019) 1940.
8. W. Tian, S. Li, X. Chen, J. Liu, and M. Yu, *Corros. Sci.,* 107 (2016) 211.
9. W. Tian, S. Li, B. Wang, J. Liu, and M. Yu, *Corros. Sci.,* 113 (2016) 1.
10. D. Song, A.B. Ma, J.H. Jiang, P.H. Lin and J. Shi, *Corros. Eng. Sci. Techn.,* 46 (2013) 505.
11. D. Song, A. Ma, J. Jiang, P. Lin, D. Yang and J. Fan, *Corros. Sci.,* 52 (2010) 481.
12. K.D. Ralston, D. Fabijanic and N. Birbilis, *Electrochim. Acta,* 56 (2011) 1729.
13. G. Meng, L. Wei, T. Zhang, Y. Shao, F. Wang, C. Dong and X. Li, *Corros. Sci.,* 51 (2009) 2151 .
14. S.X. Li, Y.N. He, S.R. Yu and P.Y. Zhang, *Corros. Sci.,* 66 (2013) 211.
15. O. Jilani, N. Njah and P. Ponthiaux, *Corros. Sci.,* 87 (2014) 259.
16. S. Gollapudi, *Corros. Sci.,* 62 (2012) 90.

17. L. Fan and H. Lu, *J. Power Sources*, 284 (2015) 409.
18. L. Dolega, B. Adamczyk-Cieślak, J. Mizera and K. J. Kurzydłowski, *J. Mater. Sci.,* 47 (2011) 3026.
19. J.G. Brunner, N. Birbilis, K.D. Ralston and S. Virtanen, *Corros. Sci.,* 57 (2012) 209.
20. A. Abbasi Aghuy, M. Zakeri, M. H. Moayed and M. Mazinani, *Corros. Sci.,* 94 (2015) 368.
21. Z. Zhang, S. K. Vajpai, D. Orlov and K. Ameyama, *Mater. Sci. Eng. A-Struct. Mater. Prop. Microstruct. Process.,* 598 (2014) 106.
22. T. Sekiguchi, K. Ono, H. Fujiwara and K. Ameyama, *Mater. Trans.,* 51 (2010) 39.
23. D. Orlov, H. Fujiwara and K. Ameyama, *Mater. Trans.*, 54 (2013) 1549 .
24. J. A. Lyndon, R. K. Gupta, M. A. Gibson and N. Birbilis, *Corros. Sci.,* 70 (2013) 290.
25. W. Tian, F. Chen, Z. Li, G. Pang and Y. Meng, *Corros. Sci.*, https://doi.org/10.1016/j.corsci.2020.108775.
26. F.X. Song, X.M. Zhang, S.D. Liu, Q. Tan and D.F. Li, *Corros. Sci.,* 78 (2014) 276.
27. J.C. Lin, H.L. Liao, W.D. Jehng, C.H. Chang and S.L. Lee, *Corros. Sci.*, 48 (2006) 3139.
28. M.I. Abd El Aal and M.M. Sadawy, *T. Nonferr. Metal. Soc.,* 25 (2015) 3865.
29. K. Srinivasan, and A. Kottantharayil, *Sol. Energ. Mat. Sol. C.,* 197 (2019) 93.
30. J.J. Huang, C.H. Lin, Y.R. Ho, and Y.H. Chang, *Surf. Coat. Tech.,* 23 (2020) 125684.
31. P. Schmuki and H. Böhni, *Electrochim. Acta,* 40 (1995) 775 .
32. P. Marcus, V. Maurice and H.H. Strehblow, *Corros. Sci.*, 50 (2008) 2698.
33. W. Tian , S. Li, N. Du, S. Chen, and Q. Wu, *Corros. Sci.,* 93 (2015) 242.
34. B. Hirschorn, B. Tribollet and M.E. Orazem, *Isr. J. Chem.*, 48 (2008) 133.
35. B. Hirschorn, M.E. Orazem, B. Tribollet, V. Vivier, I. Frateur and M. Musiani, *J. Electrochem. Soc.,* 157 (2010) C452.
36. B. Hirschorn, M.E. Orazem, B. Tribollet, V. Vivier, I. Frateur and M. Musiani, *J. Electrochem. Soc.,* 157 (2010) C458.
37. B. Hirschorn, M.E. Orazem, B. Tribollet, V. Vivier, I. Frateur and M. Musiani, *Electrochim. Acta,* 55 (2010) 6218.
38. B. Hirschorn and M. E. Orazem, *J. Electrochem. Soc.,* 156 (2009) C345.
39. S. Marcelin, B. Ter-Ovanessian and B. Normand, *Electrochem. Commun.,* 66 (2016) 62.
40. S.P. Harrington and T.M. Devine, *J. Electrochem. Soc.*, 156 (2009) C154.
41. M. Benoit, C. Bataillon, B. Gwinner, F. Miserque, M.E. Orazem, C.M. Sanchez-Sanchez, B. Tribollet and V. Vivier, *Electrochim. Acta,* 201 (2016) 340.
42. A. Fattah-alhosseini, M.A. Golozar, A. Saatchi and K. Raeissi, *Corros. Sci.,* 52 (2010) 205.
43. M. Pilaski and M.M. Lohrengel, *Electrochim. Acta,* 48 (2003) 1309.
44. J. Evertsson, F. Bertram, F. Zhang, L. Rullik, L.R. Merte, M. Shipilin, M. Soldemo, S. Ahmadi, N. Vinogradov, F. Carla, J. Weissenrieder, M. Gothelid, J. Pan, A. Mikkelsen, J.O. Nilsson and E. Lundgren, *Appl. Surf. Sci.*, 349 (2015) 826.
45. S. Ningshen, U.K. Mudali, V.K. Mittal and H.S. Khatak, *Corros. Sci.*, 49 (2007) 481